UDK: 544.3.01+546.55'22/23

PHASE EQUILIBRIA IN THE Cu_8SiS_6- Cu_8SiSe_6 SYSTEM AND CHARACTERIZATION OF THE SOLID SOLUTIONS $Cu_8SiS_{6-x}Se_x$

L.F.Mashadiyeva[1*], A.N.Poladova[2], G.F.Hasanov[1], U.R.Bairamova[3], M.B.Babanly[2]

[1]Baku State University, Baku, Azerbaijan
[2]Institute of Chemistry Public Legal Entity, MSE RA, Baku, Azerbaijan
[3] Baku Engineering University, Baku, Azerbaijan

*leylafm76@gmail.com

Received 29.04.2026
Reviewed 01.06.2026
Accepted 01.08.2026

Argyrodite-family compounds are environmentally friendly functional materials that exhibit valuable properties, including thermoelectric, photoelectric, and optical characteristics, as well as significant ionic conductivity owing to the high mobility of Ag^+ and Cu^+ ions. In this study, the phase equilibria in the Cu_8SiS_6–Cu_8SiSe_6 argyrodite system were investigated using differential thermal analysis, X-ray phase analysis, scanning electron microscopy, and microhardness measurements. It was established that the system is quasi-binary in nature and is characterized by the formation of a continuous solid-solution series (δ-phase) between the high-temperature modifications of the initial compounds, whereas broad solid-solution regions with extensive homogeneity ranges form based on their low-temperature modifications. The formation of solid solutions is accompanied by a decrease in the polymorphic transformation temperatures of the initial phases, resulting in the stabilization of the high-temperature δ-phase at room temperature over a broad composition range of 30–75 mol% Cu_8SiSe_6. The crystal lattice parameters of the synthesized solid solutions were determined, and their linear dependence on composition in accordance with Vegard's law was established.

Keywords: *copper silicon sulfide, copper silicon selenide, argyrodite-like compounds, phase equilibria, polymorphic transformation, solid solutions.*

https://doi.org/10.59849/0005-2531.2026.4.53

Introduction

Copper- and silver-based chalcogenide compounds have been intensively investigated in recent years owing to their diverse functional properties. These compounds exhibit promising thermoelectric, photoelectric, optical, ionic conductivity, and other functional properties, making them attractive for a wide range of applications, including energy conversion, optoelectronics, sensor technologies, and solid-state electrolytes [1–4]. Among these materials, argyrodite-type compounds with the general formula $A_8B^{IV}X_6$ (A = Cu, Ag; B^{IV} = Si, Ge, Sn; X = S, Se, Te) are of particular interest [5–8]. Argyrodites are characterized by a rigid anionic framework composed of tetrahedrally coordinated $[BX_4]$ structural units and a partially disordered sublattice of highly mobile Cu^+ or Ag^+ cations located within this framework. This distinctive crystal-structural feature provides these compounds with important functional advantages, including high ionic conductivity, low lattice thermal conductivity, and favorable optical and thermoelectric properties [9–12].

One of the characteristic features of the argyrodite family is the occurrence of polymorphic phase transformations at relatively low temperatures, typically below 530 K. The

low-temperature modifications crystallize in various low-symmetry ordered crystal structures, whereas the high-temperature modifications exhibit highly symmetric cubic structures [13]. With increasing temperature, the degree of disorder in the cation sublattice increases, facilitating ion migration and resulting in superionic conductivity in the high-temperature phases [14,15]. The combination of these unique structural and physical properties broadens the prospects for the application of argyrodite compounds in various modern technologies. They are considered promising functional materials for solid-state electrolytes, ion-selective electrodes, solid-state battery components, thermoelectric energy-conversion materials, as well as photoelectric and optoelectronic devices [16–20]. Furthermore, recent studies have demonstrated that cationic and anionic substitutions in these compounds can promote the formation of broad homogeneity ranges and enhance the stabilization of the crystal structure [21–36].

Solid solutions formed as a result of isovalent substitutions in argyrodite systems are of considerable scientific importance not only for understanding phase equilibria but also for the design of new functional materials. In this regard, the Cu_8SiS_6-Cu_8SiSe_6system can be considered a suitable model system for elucidating the regularities of anion substitution in silicon-based argyrodites.

Taking the above considerations into account, the present work aimed to investigate the phase equilibria in the Cu_8SiS_6-Cu_8SiSe_6 system, determine the regularities governing solid-solution formation, identify new variable-composition phases, and establish the conditions for their formation. For this purpose, the phase diagram of the system was constructed, the boundaries of the homogeneity ranges were determined, and the obtained results were analyzed in relation to the crystal-chemical characteristics of the initial components.

It should be noted that the crystal structures and polymorphic transformations of Cu_8SiS_6 and Cu_8SiSe_6 have been studied in considerable detail in the literature.

The Cu_8SiS_6 compound melts congruently at 1460 K and undergoes a polymorphic phase transformation at 336 K [37–40]. Its low-temperature (**LT**) modification possesses an orthorhombic crystal structure with lattice parameters a=0.69928(6), b=0.69000(13), and c=0.97723(14) [40], and a=0.70445(3), b=0.69661(3), and c=0.98699(5) [41]. In contrast, the high-temperature (**HT**) modification crystallizes in a cubic lattice ($F\bar{4}3m$) with a=0.976 [40] and a=0.981 [42].

The Cu_8SiSe_6 compound melts congruently at 1380 K and undergoes a polymorphic transformation at 335 K [38,42]. Its low-temperature modification has an orthorhombic crystal structure ($Pmn2_1$, a=0.72835(2), b=0.72185(2), c=1.02281(3) [40]), whereas the high-temperature modification is characterized by a cubic crystal structure ($F\bar{4}3m$, a=1.017 Å) [42].

Experimental Part

High-purity Cu, Si, S, and Se elements (at least 99.999 wt.% purity) were used for the synthesis of the initial argyrodite compounds. The elements were melted in evacuated quartz ampoules. To prevent the reaction of silicon with quartz at elevated temperatures, the inner surfaces of the ampoules were precoated with graphite.

The synthesis was carried out in an inclined two-zone furnace consisting of hot and cold zones, taking into account the high vapor pressures of sulfur and selenium. The temperature of the hot zone, located in the lower part of the furnace, was maintained at approximately 1300 K, whereas the temperature of the cold zone was set 50–100 K below the boiling point of the corresponding chalcogen. Sulfur or selenium vapors condensed in the cold zone and subsequently returned to the reaction zone. After most of the chalcogen had reacted, the ampoule was completely placed inside the furnace and maintained at this temperature for 2–3 h, after which it was cooled to room temperature in the switched-off furnace.

The synthesized compounds were identified by differential thermal analysis (DTA) and X-ray phase analysis (XPA). According to the DTA results, the polymorphic transformation and melting temperatures were determined to be 336 and 1460 K for Cu_8SiS_6 and 335 and 1380 K for Cu_8SiSe_6, respectively. These values are consistent with the literature data [26,30]. The X-ray diffraction results demonstrated that the crystal lattice parameters of the synthesized compounds are in good agreement with those reported in previous studies [24, 26].

Alloys of the Cu_8SiS_6-Cu_8SiSe_6 system were prepared by jointly melting stoichiometric amounts of the previously synthesized and identified initial compounds in evacuated quartz ampoules. To achieve equilibrium, the samples were annealed at 800 K for 500 h. Two series of samples were prepared for each composition. The first series was slowly cooled in the furnace after heat treatment, whereas the second series was rapidly quenched from 800 K by immersing the ampoules in cold water. The prepared samples were subsequently investigated by DTA and XPA.

Differential thermal analysis was performed using a NETZSCH 404 F1 Pegasus instrument and a multichannel DTA setup based on a TC-08 Thermocouple Data Logger. The temperature measurement accuracy was ±2 K. The thermal analysis data were processed using NETZSCH Proteus software.

X-ray phase analysis was performed at room temperature using $CuK\alpha_1$ radiation over the $2\theta = 5–75°$ range on a Bruker D2 PHASER diffractometer. The obtained diffraction patterns were processed using TOPAS V3.0 software, and the crystal lattice parameters were determined.

Results and discussion

X-ray phase analysis of the samples annealed at 800 K showed that all the samples exhibit diffraction patterns characteristic of the cubic crystal system. The X-ray diffraction patterns of both the initial compounds and the alloys of the investigated system were indexed, and their crystal lattice parameters were calculated. The obtained results are presented in Table 2.

At the initial stage of the study, both the samples were slowly cooled after heat treatment, and the annealed samples were investigated by X-ray phase analysis. It was established that the alloys in the composition range of 30–60 mol% Cu_8SiSe_6 exhibit diffraction patterns qualitatively different from those of the initial compounds and can be indexed in a cubic crystal structure with the $F\bar{4}3m$ space group. The diffraction pattern of the sample containing 20 mol% Cu_8SiSe_6 is identical to that of pure RT- Cu_8SiS_6, whereas the diffraction pattern of the sample containing 90 mol% Cu_8SiSe_6 coincides with that of pure RT- Cu_8SiSe_6. The diffraction pattern of the sample with a composition of 80 mol% Cu_8SiSe_6 consists of a superposition of diffraction lines corresponding to orthorhombic and cubic phases.

Thus, the results of the X-ray phase analysis demonstrate that a cubic δ-solid-solution phase forms at room temperature in the composition range of 30–60 mol% Cu_8SiSe_6. The solubility based on Cu_8SiS_6 exceeds 10 mol%, whereas that based on Cu_8SiSe_6 is approximately 10 mol%.

As shown in Figure 2, the dependence of the cubic lattice parameter on composition is linear in both systems and follows Vegard's law. In addition, the lattice parameters of the cubic phase determined for the samples annealed at 800 K are slightly larger than the corresponding values measured at room temperature. This difference can be attributed to the thermal expansion of the crystal lattice with increasing temperature.

Based on a comprehensive analysis of the DTA and XRD results, the phase diagram of the Cu_8SiS_6-Cu_8SiSe_6 system was constructed (Fig.3). A systematic interpretation of the experimental data made it possible to establish the phase equilibria in the system, determine the nature of the phase transformations, and elucidate the crystallization behavior of alloys with different compositions.

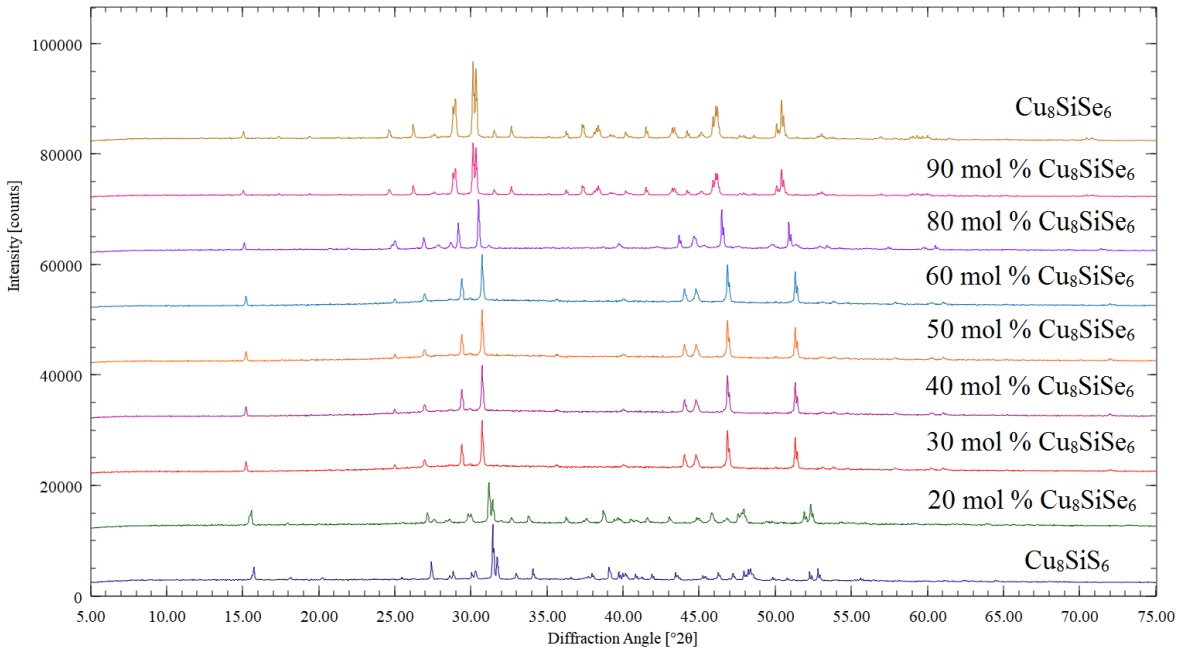


Fig.1. Powder X-ray diffraction patterns of selected alloys of the Cu_8SiS_6-Cu_8SiSe_6 system slowly cooled after annealing.

Table 1. Crystallographic parameters of phases in the Cu_8SiS_6-Cu_8SiSe_6 system

Composition, mol % Cu_8SiSe_6	**Crystal structure, Sp.gr., lattice parameters, nm**	
	Slowly cooled alloys	**Quenched from 800 K**
0(Cu_8SiS_6)	Ortorombic, *Pmn*21, a=0.69928(6), b=0.69000(13), c=0.97723 (14)	Cubic, $F\bar{4}3m$, *a* = 0.976
20	Ortorombic, *Pmn*21, a=0.7051, b=0.6962, c =0.9863	-"-, *a*=0.9851(6)
30	Cubic, $F\bar{4}3m$, *a*=0.9859(5)	
40	-"-, *a*=0.9895(7)	-"-, *a*=0.9942(6)
50	-"-, *a*=0.995(6)	
60	-"-, *a*=0.9981(5)	-"-, *a*=1.004(5)
70	-"-, *a*=1.0034	
80	Two phase: orthorhombic+cubic	-"-, *a*=1.0102(6)
90	Ortorombic, $Pmn2_1$, a=0.7228, b=0.7151, c =1.0134	
100(Cu_8SiSe_6)	Ortorombic, $Pmn2_1$, *a*=0.72835 (2), *b*=0.72185(2), *c*=1.02281 (3)	-"-, *a* = 1.017

Analysis of the phase diagram shows that the investigated system is quasi-binary and is characterized by the formation of a continuous solid-solution series (δ-phase) between the high-temperature cubic modifications of the initial Cu_8SiS_6 and Cu_8SiSe_6 compounds. The temperatures along the liquidus and solidus curves vary regularly and monotonically between the melting temperatures of the initial compounds over the entire composition range of the system. This indicates a high degree of mutual solubility between the components and their ability to form a common crystal structure in the high-temperature phases.

The formation of solid solutions results in a shift of the polymorphic transformation temperatures characteristic of the initial compounds toward lower temperatures. Since

the phase transformations corresponding to samples with compositions in the range of 30–70 mol% Cu_8SiSe_6 occur below room temperature, they are not detected on the DTA curves. Therefore, the corresponding phase boundaries are represented by dashed lines in the phase diagram.

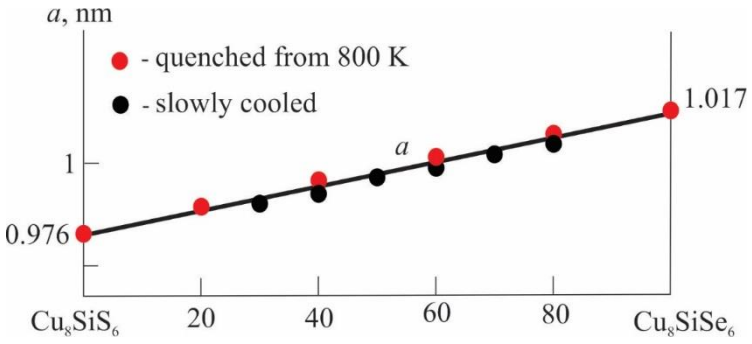


Fig.2. Dependence of the cubic lattice parameter of the Cu_8SiS_6-Cu_8SiSe_6 system on composition.

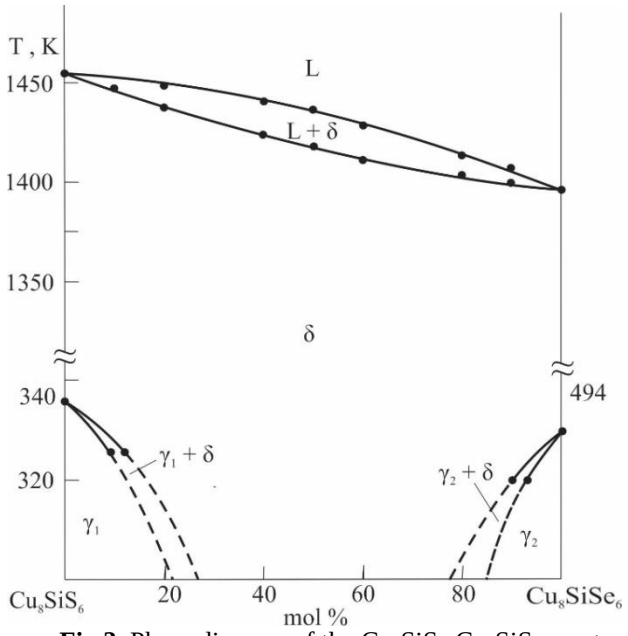


Fig.3. Phase diagram of the Cu_8SiS_6-Cu_8SiSe_6 system

The nature of the phase equilibria in the Cu_8SiS_6–Cu_8SiSe_6 system was confirmed by scanning electron microscopy (SEM). As an example, Figure 4 presents SEM micrographs of the heat-treated and slowly cooled alloys containing 10, 25, and 40 mol% Cu_8SiSe_6. As can be seen, the alloy containing 25 mol% Cu_8SiSe_6 exhibits a two-phase microstructure, whereas the alloys containing 10 and 40 mol% Cu_8SiSe_6 are single-phase, consisting of the γ_1 and δ phases, respectively.

The obtained microhardness data are presented in Figure 5 as the dependence of microhardness on composition (HV0.1–x). As can be seen, the microhardness of the cubic solid solutions increases compared with that of the initial phases, forming a broad maximum characteristic of systems in which unlimited substitutional solid solutions (δ) are formed. The measurements showed that, for slowly cooled alloys rich in the initial compounds, the composition dependence of microhardness

exhibits a somewhat different behavior. The microhardness of the room-temperature modifications of the solid solutions (shown by black circles in Figure 5) increases over a certain composition range and remains nearly constant within the two-phase regions.

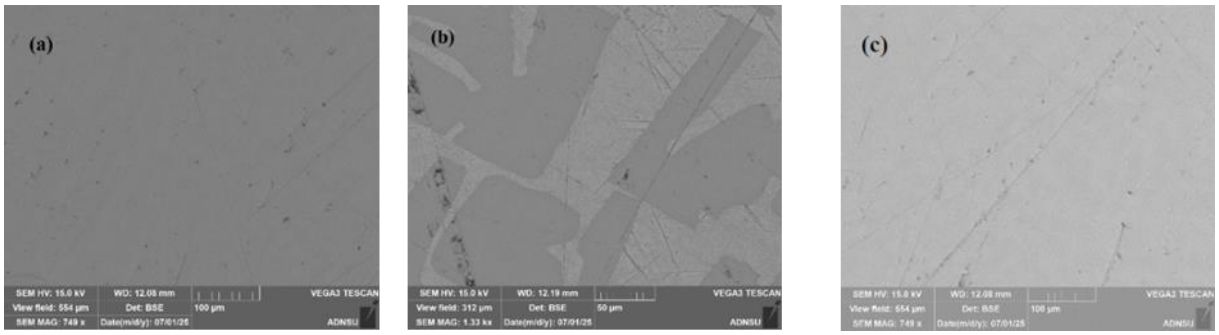


Fig.4. SEM images of alloys with compositions of 10 (a), 25 (b) and 40 (c) mol% Cu_8SiSe_6.

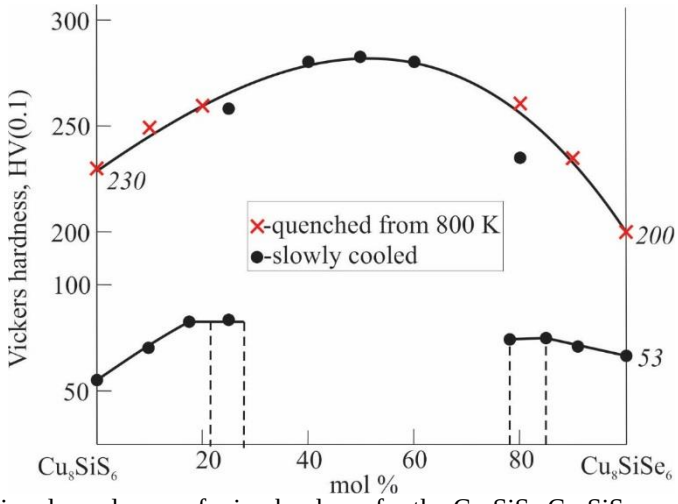


Fig.5. Concentration dependences of microhardness for the Cu_8SiS_6-Cu_8SiSe_6 system

Conclusions

The phase equilibria in the Cu_8SiSe_6 - Cu_8SiSe_6 system were systematically investigated using differential thermal analysis and X-ray phase analysis, and a temperature–composition (T–x) phase diagram was constructed based on the experimental results. It was established that the system is quasi-binary and that continuous substitutional solid solutions form between the high-temperature modifications of the initial compounds. The formation of solid solutions was shown to result in a decrease in the polymorphic transformation temperatures, leading to the stabilization of the ion-conducting cubic δ-phase at room temperature and below over the composition range of 30–75 mol% Cu_8SiSe_6.

The X-ray phase analysis results confirmed that the crystal lattice parameters of the synthesized solid solutions exhibit a linear dependence on composition, consistent with Vegard's law. The obtained results contribute to a deeper understanding of the phase relationships in the Cu_8SiSe_6-Cu_8SiSe_6 system. The synthesized solid solutions may be considered environmentally friendly and promising functional materials with potentially high thermoelectric properties and mixed ionic–electronic conductivity.

References

1. Wei T.R., Qiu P., Zhao K. et al. Ag_2Q-based (Q = S, Se, Te) silver chalcogenide thermoelectric materials. *Adv. Mater.* 2023. V. 35. № 1. P. 2110236. doi.org/10.1002/adma.202110236
2. Khan M.E., Aslam J. *Metal-Chalcogenide Nanocomposites: Fundamentals, Properties and Industrial Applications*. Woodhead Publishing. 2023.
3. Kumar A., Gupta R.K. *2D Semiconducting Materials for Electronic, Photonic, and Optoelectronic Devices*. CRC Press. 2024. doi.org/10.1201/9781003439448
4. Alfred M.O., Akor E., Ayeni B.C. et al. Chalcogenides: recent advances in their environmental applications. *Energ. Ecol. Environ.* 2026. V. 11. P. 10–38. doi.org/10.1007/s40974-025-00389-1
5. Parashchuk T., Cherniushok O., Wiendlocha B. et al. High thermoelectric performance in low-cost $Cu_8SiS_xSe_{6-x}$ argyrodite. *Adv. Funct. Mater.* 2025. V. 35. № 34. P. 2502163. doi.org/10.1002/adfm.202502163
6. Ghata A., Eckert P.L., Böger T. et al. Influence of Cu^+ substitution on the structural, ionic, and thermal transport properties of $Ag_{8-x}Cu_xGeS_6$ argyrodites. *Chem. Mater.* 2025. V. 37. № 12. P. 6900–6911. doi.org/10.1021/acs.chemmater.5c01679
7. Lin S., Li W., Pei Y. Thermally insulative thermoelectric argyrodites. *Mater. Today*. 2021. V. 48. P. 198. doi.org/10.1016/j.mattod.2021.01.007
8. Pogodin A.I., Filep M.J., Izai V.Yu., et al. Crystal growth and electrical conductivity of Ag_7PS_6 and Ag_8GeS_6 argyrodites. *J. Phys. Chem.* Solids. 2022. V. 168. P. 110828. doi.org/10.1016/j.jpcs.2022.110828.
9. Kuhs W.F., Nitsche R., Scheunemann K. The argyrodites — A new family of tetrahedrally close-packed structures. *Mater. Res. Bull.* 1979. V. 14. № 2. P. 241–248. doi.org/10.1016/0025-5408(79)90125-9
10. Bindi L., Biagioni C. A crystallographic excursion in the extraordinary world of minerals: the case of Cu- and Ag-rich sulfosalts. *Acta Crystallogr. B: Struct. Sci. Cryst. Eng. Mater.* 2018. V. 74. P. 527–538. doi.org/10.1107/S2052520618014452
11. Ren Q., Gupta M.K., Jin M. et al. Extreme phonon anharmonicity underpins superionic diffusion and ultralow thermal conductivity in argyrodite Ag_8SnSe_6. *Nat. Mater.* 2023. V. 22. P. 999–1006. doi.org/10.1038/s41563-023-01560-x
12. Wei P.-Ch., Hsing Ch.-R., Yang Ch.-Ch. et al. Liquid-like thermal conductivity in solid materials: Dynamic behavior of silver ions in argyrodites. *Nano Energy*. 2024. V. 122. P. 109324. doi.org/10.1016/j.nanoen.2024.109324
13. Babanly M.B., Yusibov Yu.A., Imamaliyeva S.Z. et al. Phase diagrams in the development of the argyrodite family compounds and solid solutions based on them. *J. Phase Equilib. Diffus.* 2024. V. 45. № 3. P. 228–255. doi.org/10.1007/s11669-024-01088-w
14. Shen X., Koza M.M., Ouyang N. et al. Soft phonon mode triggering fast Ag diffusion in superionic argyrodite Ag_8GeSe_6. *Small*. 2023. V. 19. № 49. P. 2305048. doi.org/10.1002/smll.202305048
15. Kang T., Li C., Zhang X. et al. Local symmetry breaking induced superionic conductivity in argyrodites. *J. Am. Chem. Soc.* 2026. V. 148. № 6. P. 6158–6166. doi.org/10.1021/jacs.5c17193
16. Lin S., Hou Y., Yang J. et al. Enhanced weighted mobility-induced high thermoelectric performance in argyrodite Ag_8SnSe_6. *ACS Appl. Mater. Interfaces*. 2024. V. 16. № 43. P. 58912–58919. doi.org/10.1021/acsami.4c14311
17. Dallas P., Tzitzios V.K., Givalou L. et al. Effects of ligand coordination on Ag_8SnS_6 as a photoabsorber for thin film solar cells. *J. Mater. Chem. C*. 2025. V. 13. P. 7996–8005. doi.org/10.1039/D5TC00397K
18. Bustamante J., Ghata A., Naik A.A. et al. Thermal transport in Ag_8TS_6 (T = Si, Ge, Sn) argyrodites: An integrated experimental, quantum-chemical, and computational modelling study. *J. Mater. Chem. A*. 2026. https://doi.org/10.48550/arXiv.2510.23133
19. Jiang Q., Li S., Yubo L. et al. Eco-friendly, highly robust Ag_8SiSe_6-based thermoelectric composites with excellent performance near room temperature. *ACS Appl. Mater. Interfaces*. 2020. V. 12. № 49. P. 54653–54661. https://doi.org/10.1021/acsami.0c15877
20. Munsif M., Shah M., Murtaza G. et al. First-principles study of silver argyrodites-structured compounds A_8BC_6 (A = Ag; B = Si, Ge; C = Te) for optoelectronic application. *J. Chem. Environ.* 2023. V. 1. P. 40–51. doi.org/10.56946/jce.v1i02.121
21. Mashadiyeva L.F., Babanly D.M., Poladova A.N., Yusibov Y.A., Babanly M.B. Liquidus surface and phase relations in the Cu-Sb-S system. *Properties and Uses of Antimony.* 2022, P. 45–72. https://doi.org/10.52305/OJKB5395.
22. Huseynova I.F., Bayramova N.A., Imamaliyeva S.Z. et al. Phase equilibria in the Ag_8GeSe_6–Ag_7GeSe_5I–$GeSe_2$ system. *Russ. J. Inorg. Chem.* 2025. V. 70. № 11. P. 1793–

1802. https://doi.org/10.7868/S3034560X25110207
23. Bayramova U.R., Poladova A.N., Mashadiyeva L.F. Synthesis and X-ray study of the $Cu_8Ge_{1-x}Si_xS_6$ solid solutions. *New Mater. Compd. Appl.* 2022. V. 6. № 3. P. 276–281.
24. Bairamova U.R., Babanly K.N., Mashadieva L.F. et al. Phase equilibria in the Cu_2Se–Cu_8SiSe_6–Cu_8GeSe_6 system. *Russ. J. Inorg. Chem.* 2023. V. 68. № 11. P. 1611–1621. https://doi.org/10.1134/S0036023623602027
25. Ashirov G.M., Babanly K.N., Mashadiyeva L.F. et al. Phase equilibria in the Ag_2S–Ag_8GeS_6–Ag_8SiS_6 system and some properties of solid solutions. *Condens. Matter Interphases*. 2023. V. 25. № 2. P. 292–301. doi.org/10.17308/kcmf.2023.25/11168
26. Bayramova U.R., Babanly K.N., Ahmadov E.I. et al. Phase equilibria in the Cu_2S–Cu_8SiS_6–Cu_8GeS_6 system and thermodynamic functions of phase transitions of the $Cu_8Si_{1-x}Ge_xS_6$ argyrodite. *J. Phase Equilib. Diffus.* 2023. V. 44. № 3. P. 509–519. https://doi.org/10.1007/s11669-023-01054-y
27. Poladova A.N., Huseynova I.F., Alverdiyev I.J. et al. Cu_8GeSe_6–Ag_8GeS_6 system: Phase equilibria and high-entropy alloys. *Russ. J. Inorg. Chem.* 2025. V. 70. № 11. P. 1779–1785. https://doi.org/10.1134/S0036023625602132
28. Ashirov G.M., Babanly K.N., Mashadiyeva L.F. et al. Phase equilibria in the Ag_2Se–Ag_8GeSe_6–Ag_8SiSe_6 system and characterization of the $Ag_8Si_{1-x}Ge_xSe_6$ solid solutions. *Chem. Probl.* 2023. V. 21. № 3. P. 229–241. doi.org/10.32737/2221-8688-2023-3-229-241
29. Poladova A, Namazov J, Mashadiyeva L, Yusibov Y, Babanly M. Phase Behavior in Cu_8SiS_6- Ag_8SiS_6 and Cu_8SiSe_6-Ag_8SiSe_6 Systems and New Cubic Argyrodite Phases with Variable Composition. JOTCSA. 2026; 2026(2):1941935, 1-9. https://doi.org/10.18596/jotcsa.1941935
30. Poladova A.N., Aliyeva A.Sh., Mashadiyeva L.F., et al. Phase equılıbrıa and hıgh-entropy alloys ın the Cu_8SiS_6–Ag_8SiSe_6 system. *Russ. J. Inorg. Chem.* 2026. V. 71. № 10. P. 1625–1634.
31. Alverdiev I.J., Bagheri S.M., Aliyeva Z.M. et al. Phase equilibria in the Ag_2Se–$GeSe_2$–$SnSe_2$ system and thermodynamic properties of $Ag_8Ge_{1-x}Sn_xSe_6$ solid solutions. *Inorg. Mater.* 2017. V. 53. P. 786–? . https://doi.org/10.1134/S0020168517080027
32. Imamaliyeva S.Z., Abbasova V.A., Huseynova I.F., et al. Phase equilibria in the Cu_2Se-Ag_2Se-$GeSe_2$ system, crystallization and thermodynamic properties of the $Cu_{8(1-x)}Ag_{8x}GeSe_6$ solid solutions, *J. Alloys Compd*. 2026. V.1080. P. 190552, https://doi.org/10.1016/j.jallcom.2026.190552.
33. Huseynova I.F., Bayramova N.A., Imamaliyeva S.Z., et al. Phase relations and crystallisation prosesses in the Ag_2Se-AgI-$GeSe_2$ system. J. Phase Equilib. Diffuse. 2026. V.47. №3. P. 278–288.
34. Bayramova N.A., Huseynova I.F., Babanly K.N., et al. Synthesis and physicochemical study of the $Ag_{8-x}SnSe_{6-x}I_x$ solid solutions. Azerbaijan Chem. J. 2026. №3. P.37-45
35. Huseynova I.F., Bayramova N.A., Imamaliyeva S.Z. et al. Phase relations and crystallisation processes in the Ag_2Se–AgI–$GeSe_2$ system. *J. Phase Equilib. Diffus.* 2026. V. 47. № 3. P. 278–288.
36. Imamaliyeva S.Z., Abbasova V.A., Babanly K.N. et al. Phase equilibria and copper–silver-substituted solid solutions in the Cu_2S–Ag_2S–GeS_2 system. *JOM*. 2026. https://doi.org/10.1007/s11837-026-08390-7
37. Venkatraman M., Blachnik R., Schlieper A. The phase diagrams of M_2X–SiX_2 (M is Cu, Ag; X is S, Se). *Thermochim. Acta*. 1995. V. 249. P. 13–20. https://doi.org/10.1016/0040-6031(95)90666-5
38. Olekseyuk I., Piskach L., Zhbankov O. et al. Phase diagrams of the quasi-binary systems Cu_2S–SiS_2 and Cu_2SiS_3–PbS and the crystal structure of the new quaternary compound Cu_2PbSiS_4. *J. Alloys Compd*. 2005. V. 399. № 1. P. 149–154. https://doi.org/10.1016/j.jallcom.2005.03.086
39. Levalois M., Allais G. Structure du sulfure de cuivre et de silicium Cu_8SiS_6. *Acta Crystallogr. B*. 1981. V. 37. P. 1816–1819. [in French]. https://doi.org/10.1107/S0567740881007322
40. Ishii M., Onoda M., Shibata K. Structure and vibrational spectra of argyrodite family compounds Cu_8SiX_6 (X = S, Se) and Cu_8GeS_6. *Solid State Ionics*. 1999. V. 121. № 1–4. P. 11–18. https://doi.org/10.1016/S0167-2738(98)00305-1
41. Hahn H., Schulze H., Sechser L. Über einige ternäre Chalkogenide vom Argyrodit-Typ. *Naturwissenschaften*. 1965. V. 52. № 15. P. 451. [in German]. https://doi.org/10.1007/BF00627053
42. Heep B.K., Weldert K.S., Krysiak Y. et al. High electron mobility and disorder induced by silver ion migration lead to good thermoelectric performance in the argyrodite Ag_8SiSe_6. *Chem. Mater*. 2017. V. 29. № 11. P. 4833–4839. https://doi.org/10.1021/acs.chemmater.7b00767

Cu_8SiS_6–Cu_8SiSe_6 SİSTEMİNDƏ FAZA TARAZLIQLARI VƏ $Cu_8SiS_{6-x}Se_x$ BƏRK MƏHLULLARININ XARAKTERİSTİKASI

L.F. Maşadiyeva, A.N. Poladova, G.F. Həsənov, U.R. Bairamova, M.B. Babanlı

Argirodit ailəsi birləşmələri ekoloji cəhətdən təhlükəsiz funksional materiallar olub, termoelektrik, fotoelektrik və optik xassələri, həmçinin Ag^+ və Cu^+ ionlarının yüksək hərəkətliliyi ilə əlaqədar əhəmiyyətli ion keçiriciliyi ilə xarakterizə olunur. Bu tədqiqatda Cu_8SiS_6-Cu_8SiSe_6 argirodit sistemində faza tarazlıqları diferensial termiki analiz, rentgenfaza analizi, skanedici elektron mikroskopiyası və mikrobərklik ölçmələri vasitəsilə öyrənilmişdir. Müəyyən edilmişdir ki, sistem təbiətinə görə kvazibinardır və ilkin birləşmələrin yüksəktemperaturlu modifikasiyaları arasında fasiləsiz bərk məhlul sırasının **(**δ-faza**)** əmələ gəlməsi ilə xarakterizə olunur. Eyni zamanda, ilkin birləşmələrin aşağıtemperaturlu modifikasiyaları əsasında geniş homogenlik sahələrinə malik geniş bərk məhlul oblastları formalaşır. Bərk məhlulların əmələ gəlməsi ilkin fazaların polimorf çevrilmə temperaturlarının azalması ilə müşayiət olunur. Bunun nəticəsində yüksəktemperaturlu δ-fazanın otaq temperaturunda Cu_8SiSe_6-nın 30–75 mol% miqdarına uyğun geniş tərkib intervalında stabilləşməsi baş verir. Sintez edilmiş bərk məhlulların kristal qəfəs parametrləri müəyyən edilmiş və onların tərkibdən asılılığının Vegard qanununa uyğun olaraq xətti xarakter daşıdığı müəyyən olunmuşdur.

Açar sözlər: *mis-silisium sulfide, mis-silisium selenidi, arqirodit tipli birləşmələr, faza tarazlıqları, polimorf çevrilmə, bərk məhlullar.*